Available online at www.sciencedirect.com
ScienceDirect
Materials Research Bulletin 43 (2008) 3543–3552
Materials Research Bulletin
www.elsevier.com/locate/matresbu

Electrochemical behaviors of $Li[Li_{(1-x)/3}Mn_{(2-x)/3}Ni_{x/3}Co_{x/3}]O_2$ cathode series ($0 < x < 1$) synthesized by sucrose combustion process for high capacity lithium ion batteries

Gu-Yeon Kim [a,*], Seung-Beob Yi [b], Yong Joon Park [c], Ho-Gi Kim [a]

[a] *Department of Materials Science and Engineering, Korea Advanced Institute of Science and Technology, 373-1 Guseong-dong, Yuseong-gu, Daejeon 305-701, Republic of Korea*

[b] *Energy Business Division Development Team, SAMSUNG SDI, 508 Sungsung-dong, Chenan, Chungcheongnam-do 330-300, Republic of Korea*

[c] *Division of Advanced Industrial Engineering, Kyonggi University, 94-6 Yiui-dong, Yeongtong-gu, Suwon, Kyonggi-do, Republic of Korea*

Received 9 November 2007; received in revised form 21 December 2007; accepted 17 January 2008
Available online 29 January 2008

Abstract

A mixed cathode material between Li_2MnO_3 and $Li[Mn_{1/3}Ni_{1/3}Co_{1/3}]O_2$ for high capacity lithium secondary batteries was introduced in this study. It was prepared using the sucrose combustion process because this is a simple process. The oxidation states of Mn, Co and Ni ions in the pristine $Li[Li_{(1-x)/3}Mn_{(2-x)/3}Ni_{x/3}Co_{x/3}]O_2$ compounds were confirmed to be tetravalent, trivalent and divalent, respectively, via XANES measurements. Electrochemical charge/discharge studies showed that the highest first discharge capacity of 224 mAh/g was obtained in composition of $x = 0.5$ at a 0.2 C rate. The oxidation state of the Co and Ni ions in the $Li[Li_{1/6}Mn_{1/2}Ni_{1/6}Co_{1/6}]O_2$ changed to higher oxidation states, but that of the Mn ions did not change.

Keywords: A. Inorganic compounds; B. Chemical synthesis; C. XAFS (EXAFS and XANES); D. Electrochemical properties

1. Introduction

The Li-ion secondary battery industry has rapidly developed, as there have been many advances in technology regarding mobile electronic devices such as mobile phones, laptop computers and HEVs. As a cathode for lithium ion secondary batteries, $LiCoO_2$, commercialized by SONY in 1991 [1], has been widely used due to its good stability and favorable synthetic manufacturing method. The demand for high capacity and high-power batteries has grown due to the development trends of HEVs; however, the specific capacity of $LiCoO_2$ is limited to 150–160 mAh/g, which is approximately half of the theoretical capacity of 274 mAh/g.

Thus, numerous investigations have been made into the realization of high-capacity batteries using solid solution compounds between two cathodes. Hong et al. reported a solid solution of $Li[Ni_{0.20}Li_{0.20}Mn_{0.60}]O_2$ and $Li[Co_{0.50}Li_{0.167}Mn_{0.333}]O_2$ [2], and Lu et al. investigated a solid solution between $Li[Ni_{0.5}Mn_{0.5}]O_2$ and $LiCoO_2$ [3].

* Corresponding author. Fax: +82 42 869 8650.
E-mail address: antiserra@kaist.ac.kr (G.-Y. Kim).

0025-5408/$ – see front matter
doi:10.1016/j.materresbull.2008.01.011

Table 1
c/a values, lattice parameters and theoretical capacity of layered oxide compositions

	1:9	3:7	5:5	7:3	9:1
Theoretical capacity (mAh/g)	336.12	321.15	307.46	294.89	283.30
a (Å)	2.83700(14)	2.84947(3)	2.85330(1)	2.85806(0)	2.86248(0)
c (Å)	14.24141(65)	14.22449(25)	14.22872(11)	14.23524(0)	14.23820(4)
c/a	5.01988	4.99198	4.98676	4.98074	4.97408

Moreover, a $Li[Li_{1/3-2x/3}Mn_{2/3-x/3}Ni_x]O_2$ solid solution between Li_2MnO_3 and $Li[Mn_xNi_{1-x}]O_2$ is known to be a high capacity cathode material [4,5,6,7].

Recently, investigations of solid solutions between Li_2MnO_3 and other cathode materials have been reported [8]. There are two advantages of a solid solution between Li_2MnO_3 and other layered cathode materials. First, the theoretical capacity increases when using a light Li ion in place of heavy ions such as Co, Ni and Mn in the transition metal layer. The theoretical capacity related to this substitution is shown in Table 1. Second, the Li ions in the layered cathodes cannot be fully extracted out of the active materials due to the overlap of the $Co^{3+/4+}$:t_{2g} band by the top of the O^{2-}:2p band; therefore, the oxygen is volatilized from the lattice at a deep degree of charge (>50%), which results in a structural distortion from hexagonal to monoclinic. This can be overcome by a substitution of Co for Mn and Ni [9].

In the present work, mixed compounds of $Li[Li_{1-x/3}Mn_{2-x/3}Ni_{x/3}Co_{x/3}]O_2$, as composed of Li_2MnO_3 and $Li[Ni_{1/3}Co_{1/3}Mn_{1/3}]O_2$ were synthesized via a SCP (Sucrose Combustion Process) method. Compared with other synthetic methods, this method is very simple and involves less manufacturing time. The structural and electrochemical properties were investigated using X-ray diffraction, a charge–discharge method and XANES. In consequence, the most feasible composition of x in $Li[Li_{1-x/3}Mn_{2-x/3}Ni_{x/3}Co_{x/3}]O_2$ for the highest discharge capacity and the redox mechanism were formulated.

2. Experimental

Mixed compounds $Li[Li_{(1-x)/3}Mn_{(2-x)/3}Ni_{x/3}Co_{x/3}]O_2$ composed of $Li[Ni_{1/3}Co_{1/3}Mn_{1/3}]O_2$ and Li_2MnO_3 were prepared by a SCP method from $LiNO_3$, $Mn(NO_3)_2{\cdot}6H_2O$, $Ni(NO_3)_2{\cdot}6H_2O$ and $Co(NO_3)_2{\cdot}6H_2O$ as precursors. Initially, to make each $Li[Ni_{1/3}Co_{1/3}Mn_{1/3}]O_2$ and Li_2MnO_3 solution, stoichiometric amounts of source materials of Ni, Co, Mn and Li (molar ratio of Li:Ni:Co:Mn = 3:1:1:1 for $Li[Ni_{1/3}Co_{1/3}Mn_{1/3}]O_2$ and Li:Mn = 2:1 for Li_2MnO_3) were dissolved and mixed homogeneously in distilled water. The two solutions were mixed with ratios of 1:9, 3:7, 5:5, 7:3 and 9:1 (x = 0.1, 0.3, 0.5, 0.7 and 0.9, respectively). A powder, similar in appearance to gray ash, was produced through stirring the mixed solution continuously at 100 °C with 1 M ratio of sucrose, followed by gelation and combustion of mixed solution. The decomposed powder was ground and heated at 900 °C in a box type furnace for 12 h. It was then poured into liquid nitrogen and quenched. And the quenched powder was dried at 120 °C to evaporate the residual moisture. The synthesized particle size was measured with Malvern Mastersize S. X-ray diffraction experimental was performed using Automated Rigaku X-ray diffractometer in the 2θ ranges from 10° to 70° with Cu Kα radiation. To prepare the positive electrode, the produced powder, carbon black (Vulcan XC-72) as conductor and PVdF were mixed in homogenizer at mass ratio of 84:8:8, respectively. And a viscous slurry was coated in aluminum foil using the doctor blade with uniform thickness of 20 μm. And the coated film was dried in vacuum oven at 100 °C. Then the 2032 type coin cell was assembled in glove box filled with Ar gas using cathode film, lithium foil (Foote Mineral Co.), separator (PP, Celgard Inc.) and electrolyte (1 M $LiPF_6$ solution in a 1: 1 volume ratio of EC and DEC). Galvanostatic charge/discharge tests were performed using WBCS3000 system. The current density was 0.2 C-rate and cut off voltage was 2.0–4.8 V. The cyclic voltammograms tests were conducted from 2.0 to 4.8 V at 0.1 mV/s scan rate. The X-ray absorption near-edge structure (XANES) analysis was carried out to examine oxidation state of Mn, Co and Ni ions and the change of their oxidation state during charge/discharge measurement.

3. Results and discussion

Fig. 1 shows X-ray diffraction patterns of the $Li[Li_{(1-x)/3}Mn_{(2-x)/3}Ni_{x/3}Co_{x/3}]O_2$ cathode materials. The XRD data is indexed with that of layered $LiCoO_2$ (α-$NaFeO_2$ type, space group R-3m, hexagonal). It has been reported that

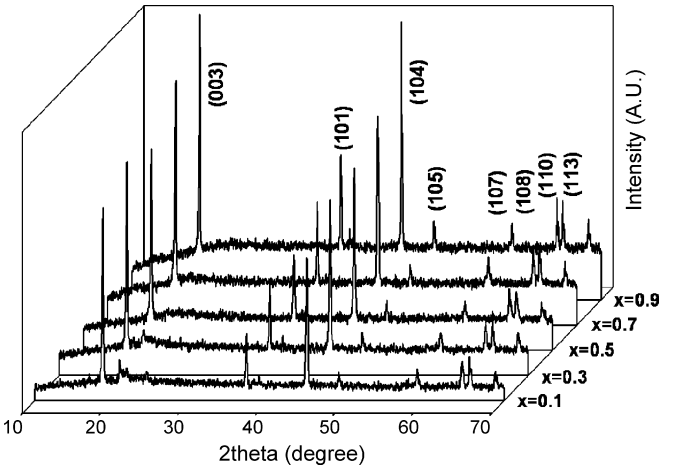

Fig. 1. XRD patterns of mixed compounds of Li_2MnO_3 and $Li[Ni_{1/3}Co_{1/3}Mn_{1/3}]O_2$.

layered structures showed a good splitting of the peaks assigned to (108, 110) with *c/a* values higher than 4.899 [10]. The clearly split (108, 110) pairs and the *c/a* ratio (when higher than 4.899) in all compositions of *x* indicate that the layered structure was synthesized successfully. The *c/a* values and lattice parameters of the $Li[Li_{(1-x)/3}Mn_{(2-x)/3}Ni_{x/3}Co_{x/3}]O_2$ are shown in Table 1.

The XRD data at compositions of $x = 0.1$ and $x = 0.3$ show superlattice peaks in the range of 21–23° which cannot be indexed to R-3m symmetry. These superlattice peaks have been considered to reflect the degree of cations ordering in the transition metal layers. According to Hackney et al. [11], Co^{3+} addition to the Li rich layered materials results in the weakening of superlattice peaks because of the increased disorder and isolation of the $LiMn_{1-x}(NiCo)_x$ domain structure. In our results of XRD, the superlattice peaks are weakened as the Co^{3+} content increased, which is consistent with the results of Hackney et al.

SEM images of $Li[Li_{(1-x)/3}Mn_{(2-x)/3}Ni_{x/3}Co_{x/3}]O_2$ are shown in Fig. 2. The particle sizes measured via Malvern Mastersize S were 1.24, 1.17, 0.84, 1.44, 1.88 and 3.04 μm at $x = 0.1$, 0.3, 0.5, 0.7, 0.9 and 1.0, respectively (data not shown). A small particle size in the cathode materials is an important factor. It greatly influences the electrochemical properties of Li-ion secondary batteries. In general, a small particle size can reduce the diffusion path of Li ions inside the particle due to the large particle/electrolyte interface, implying that Li ions inside the particle can reach the interface faster, as reported by Hinokuma et al. [12]. Therefore, the smallest particle size at $x = 0.5$ improve electrochemical characteristics such as a high rate capability.

Fig. 3 shows the initial charge/discharge curves for all compositions during the first cycle. The measurement was carried out between 2.0 and 4.8 V at a constant current density of 0.2 C rate. Two plateaus were observed at around 4.1 and 4.6 V. This figure reveals that the length of the charge plateau at 4.1 V becomes shorter as the Ni and Co contents decrease. A more detailed discussion is given below along with results of XANES.

Fig. 4(a) shows the charge/discharge capacity. The sample at $x = 0.1$ shows a low discharge capacity of 12 mAh/g, as also reported by Gopukumar and coworkers [13], and the sample at $x = 0.5$ shows the highest discharge capacity of 224 mAh/g. Thus, it was determined that the best composition for the highest discharge capacity is $x = 0.5$. The capacity retention data shown in Fig. 4(b) shows the discharge capacity ratio of the first cycle to the 10th cycle. The lowest capacity retention and the highest capacity retention are observed at $x = 1$ and $x = 0.1$, respectively. These results indicate that the structural stability of the solid solution improves as the amount of Li_2MnO_3 increases. According to Choi and Manthiram [9], cracks created by the volume change during the charge/discharge cycling of $Li[Ni_{1/3}Co_{1/3}Mn_{1/3}]O_2$ cathode can be suppressed by excessive Li ions. Therefore, capacity retention improves when the amount of Li_2MnO_3 is greater than that of $Li[Ni_{1/3}Co_{1/3}Mn_{1/3}]O_2$, as the excess Li ions from the Li_2MnO_3 play such a role in $Li[Ni_{1/3}Co_{1/3}Mn_{1/3}]O_2$. Fig. 4(b) also shows the Initial Capacity Loss (ICL), the capacity ratio of the first discharge capacity to the first charge capacity (Coulomb efficiency or Faraday efficiency). That is highest at $x = 0.1$ and lowest at $x = 1$. With $Li[Ni_{1/3}Co_{1/3}Mn_{1/3}]O_2$, a reversible reaction is dominant during charge/discharge cycling. In the case of Li_2MnO_3, however, an irreversible reaction is observed during the first charge/discharge cycle due to low coulomb efficiency, i.e., 70% of the ICL. According to Hackney et al. [11], although the Li_2MnO_3 is inactive material

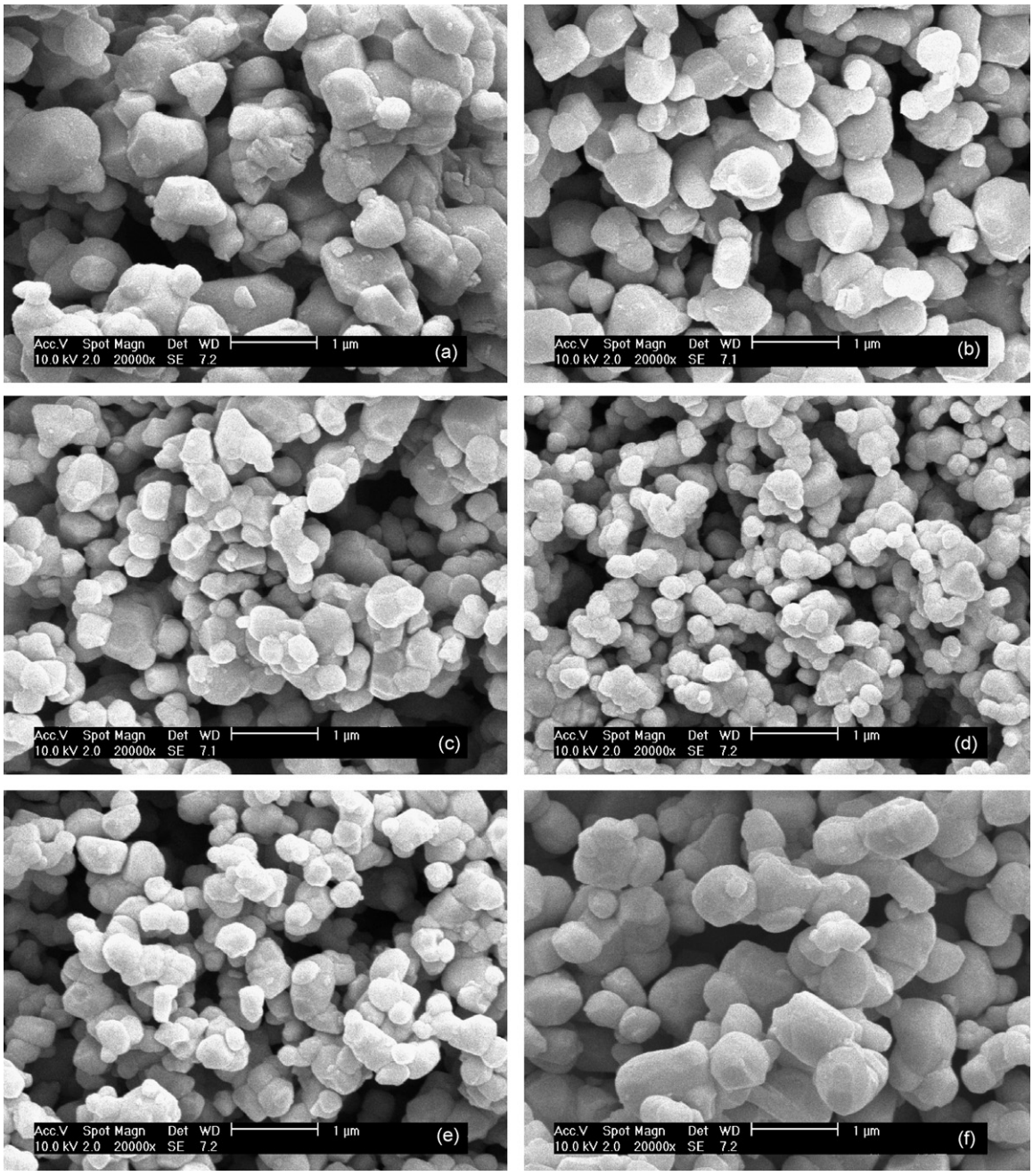

Fig. 2. SEM images of mixed compounds of Li_2MnO_3 and $Li[Ni_{1/3}Co_{1/3}Mn_{1/3}]O_2$. x = (a) 1.0, (b) 0.9, (c) 0.7, (d) 0.5, (e) 0.3 and (f) 0.1.

by itself, the Li_2MnO_3 inside a domain structure is active when the voltage is higher than 4.4 V. When charged, one Li_2MnO_3 loses one O^{2-} ion and two Li^+ ions in forms of Li_2O at above 4.4 V and becomes MnO_2. When discharged, the MnO_2 becomes $LiMnO_2$ by gaining only one Li^+ ion, which is a main reason of irreversible capacity loss on the initial cycle.

Considering the results shown in Fig. 4(a) and (b), it was determined that the optimized composition is $x = 0.5$, as the compounds of $x = 0.5$ and $Li[Li_{1/6}Mn_{1/2}Ni_{1/6}Co_{1/6}]O_2$ incorporate the advantages of both structural stability and coulomb efficiency.

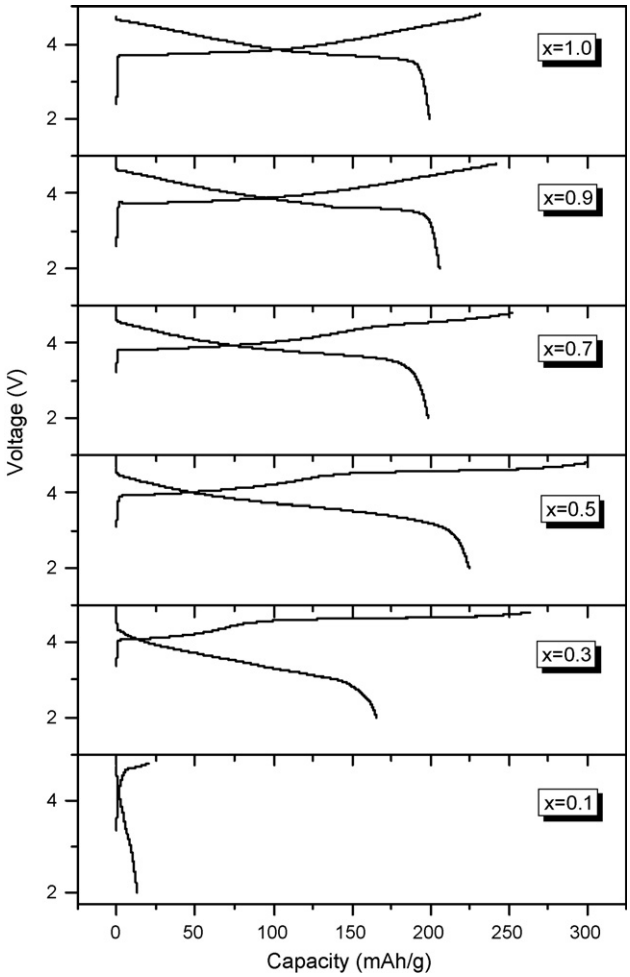

Fig. 3. First charge/discharge curves of mixed compounds of Li_2MnO_3 and $Li[Ni_{1/3}Co_{1/3}Mn_{1/3}]O_2$.

Fig. 5 shows the cyclic performance levels for the cells with the $Li[Li_{1/6}Mn_{1/2}Ni_{1/6}Co_{1/6}]O_2$ cathode material after fifty cycles between 2.0 and 4.8 V at a 0.2 C rate. $Li[Li_{1/6}Mn_{1/2}Ni_{1/6}Co_{1/6}]O_2$ compounds showed very stable cyclability. Nearly 80% discharge capacity was sustained, and the cyclability becomes more stable as the cycle proceeds. Fig. 6 shows cyclic voltammograms results measured with $Li[Li_{1/6}Mn_{1/2}Ni_{1/6}Co_{1/6}]O_2$. As shown in Fig. 6, the anodic peak at 4.6 V nearly disappears during the second charge and completely disappears after the second cycle. These results clearly show that the reaction during the 4.6 V plateau is an irreversible reaction; that is, it demonstrates the extraction of Li with O together, as reported by Dahn and coworkers [14]. In contrast, the anodic peak at 4.1 V is continues to be observed after 10 cycles. Some reversible reaction has occurred during the plateau at 4.1 V.

In order to observe these reactions during a charge/discharge process, Mn, Co and Ni K-edge XANES measurements were made of $Li[Li_{1/6}Mn_{1/2}Ni_{1/6}Co_{1/6}]O_2$ as a function of the degree of charge. The cycling curve of $Li[Li_{1/6}Mn_{1/2}Ni_{1/6}Co_{1/6}]O_2$ during two cycles is shown in Fig. 7. Representative scans are marked on the cycling curve. The region of scan 0–1 represents the plateau of 4.1 V while that of scan 2–3 represents the plateau of 4.6 V. The process was carried out with the very low current density of a 0.05C scan rate. When the charge/discharge states reached the points 0–6, respectively, the processes were stopped and the samples were collected for the XANES measurement. To observe the valence state of Mn, Co and Ni ions after especially long cycles, one sample was collected after fifty cycles. Figs. 8 and 9 show the K-edge XANES spectra of Mn, Co and Ni during first charge and during two cycles, respectively. There are references to various oxidation states of Mn, Co and Ni K-edge XANES spectra in Fig. 8(a)–(c), respectively. They indicate that the oxidation state of the Mn, Co and Ni ions of the fresh

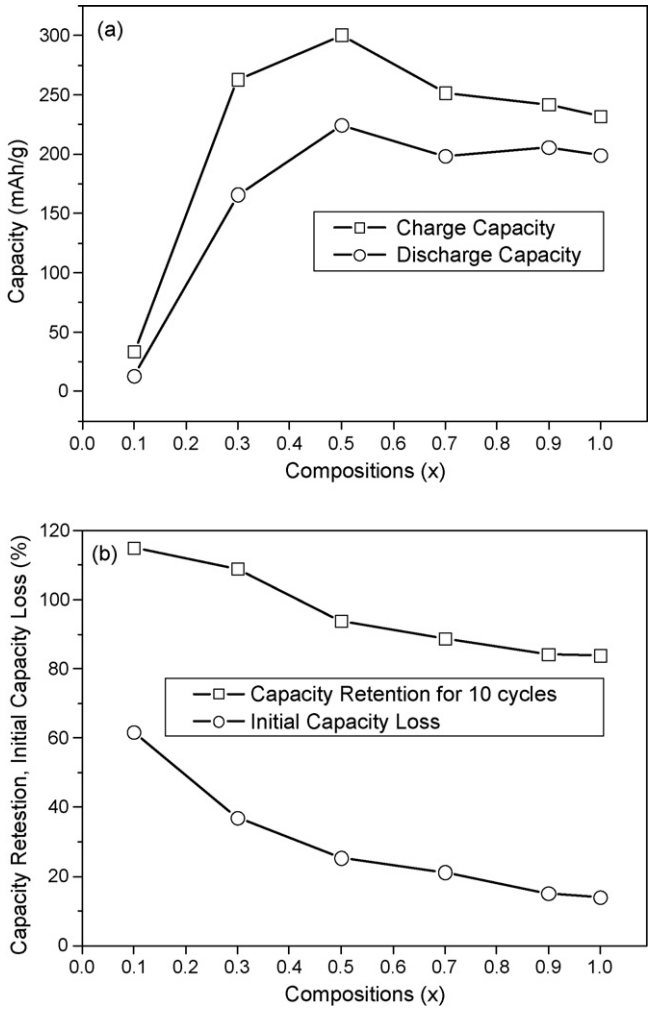

Fig. 4. (a) Electrochemical properties of mixed compounds ofLi_2MnO_3 and $Li[Ni_{1/3}Co_{1/3}Mn_{1/3}]O_2$: (□) charge capacity and (○) discharge capacity. (b) Electrochemical properties of mixed compounds of Li_2MnO_3 and $Li[Ni_{1/3}Co_{1/3}Mn_{1/3}]O_2$: (□) capacity retention and (○) initial capacity loss.

compounds (scan 0) are tetravalent, trivalent and divalent state, respectively, which corresponds to results reported by other research groups [15,16,17,18].

Fig. 8(a)–(c) shows the change of the valence state of Mn, Co and Ni ions, respectively, in the $Li[Li_{1/6}Mn_{1/2}Ni_{1/6}Co_{1/6}]O_2$ during first charge measurement. It can be seen in Fig. 8(a) that the edge shape of the Mn ions gradually changes during first charge (from scan 0 to scan 3). However, they do not show a rigid shift of the entire edge to the higher energy value. The change in the shape of the near edge spectra during the initial charge process implies that the local structural rearrangement around the Mn ions changes [17] as it is generally believed that the valence state of Mn ions in octahedral sites is tetravalent and does not during charge/discharge cycles [19]. This explains how the valence state of the Mn ions in the $Li[Li_{1/6}Mn_{1/2}Ni_{1/6}Co_{1/6}]O_2$ maintains its tetravalent status during the first charge. The edge position of the Co and Ni ions entirely shifts to a higher energy value, from 7727 to 7728.9 eV and from 8350.3 to 8354 eV, during scan 0–2, as shown in Fig. 8(b) and (c), respectively. The positive shift of the edge positions of the Co and Ni ions indicates that their oxidation states increase. From scan 2 to scan 3 (at a plateau of 4.6 V), the oxidation states of the Co and Ni ions do not change. This indicates that the plateau of 4.1 V is caused by the oxidation of the Co and Ni ions from Co^{3+} to $Co^{3.5+}$ and from Ni^{2+} to Ni^{3+}, respectively. Moreover, the plateau of 4.6 V is not affected by their oxidation.

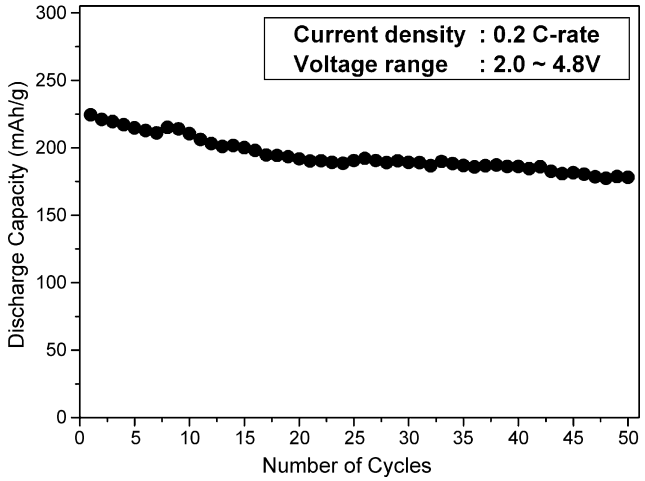

Fig. 5. Cycle performance of the $Li[Li_{1/6}Mn_{1/2}Ni_{1/6}Co_{1/6}]O_2$ compound after fifty cycles.

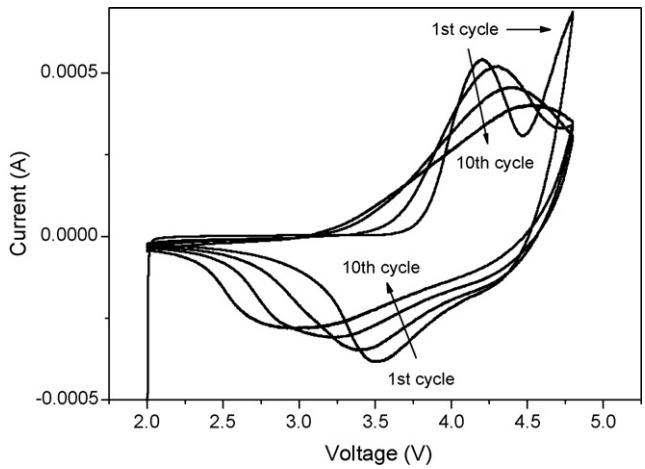

Fig. 6. Cyclic voltammograms of the $Li[Li_{1/6}Mn_{1/2}Ni_{1/6}Co_{1/6}]O_2$ compound. Scan rate is 0.1 mV/s. The voltage range is 2.0–4.8 V.

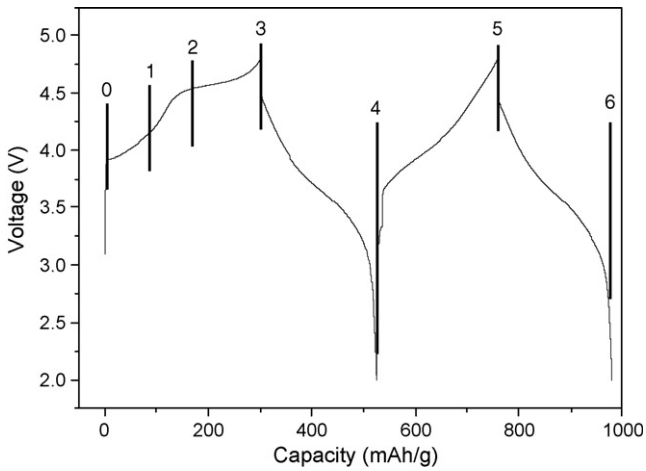

Fig. 7. Voltage profile of the cell during two cycles. Representative scans of XANES measurements are indicated.

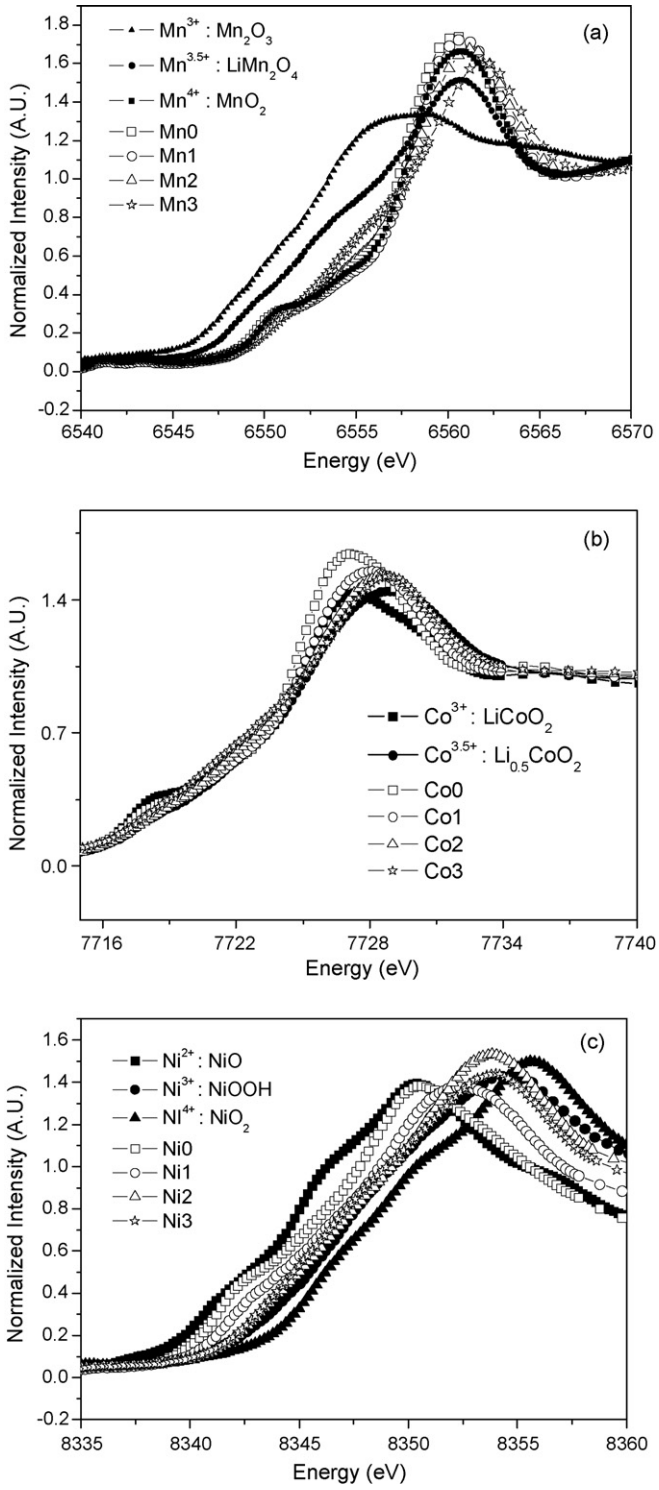

Fig. 8. (a) Mn K-edge XANES spectra for the $Li[Li_{1/6}Mn_{1/2}Ni_{1/6}Co_{1/6}]O_2$ compound during the first charge process. (b) Co K-edge XANES spectra for the $Li[Li_{1/6}Mn_{1/2}Ni_{1/6}Co_{1/6}]O_2$ compound during the first charge process. (c) Ni K-edge XANES spectra for the $Li[Li_{1/6}Mn_{1/2}Ni_{1/6}Co_{1/6}]O_2$ compound during the first charge process.

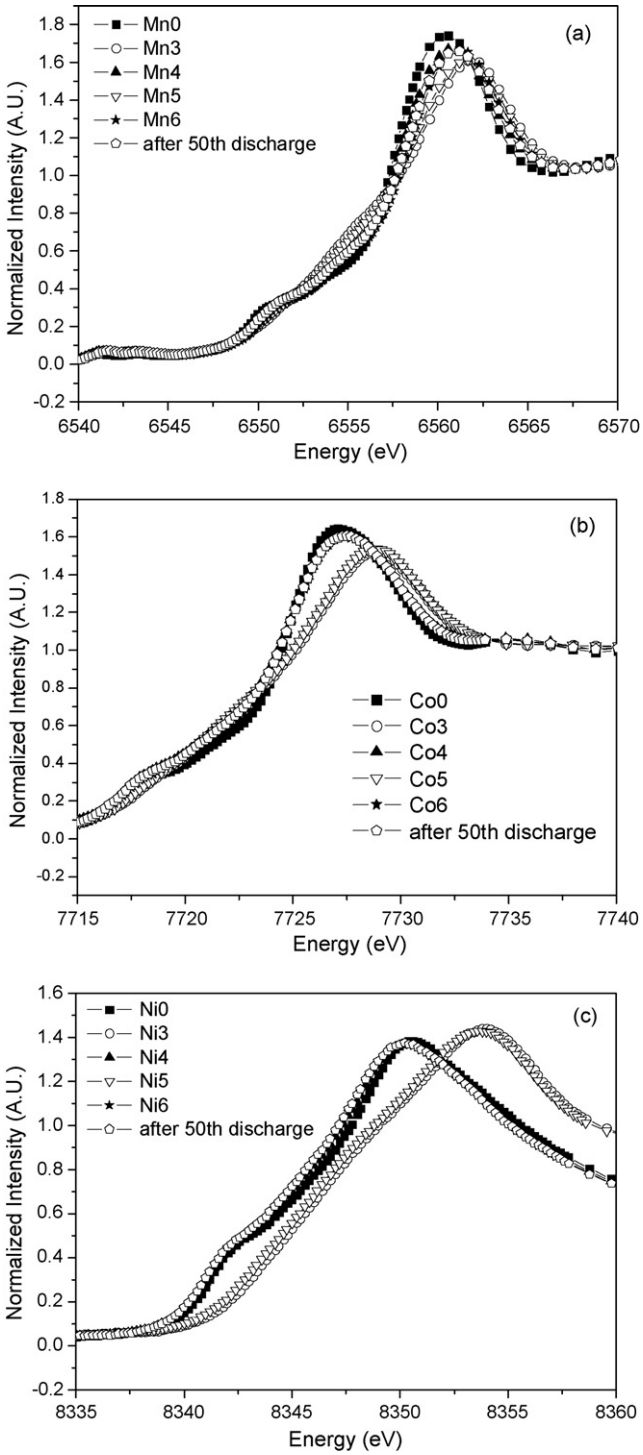

Fig. 9. (a) Mn K-edge XANES spectra for the $Li[Li_{1/6}Mn_{1/2}Ni_{1/6}Co_{1/6}]O_2$ compound during 2 cycles. (b) Co K-edge XANES spectra for the $Li[Li_{1/6}Mn_{1/2}Ni_{1/6}Co_{1/6}]O_2$ compound during 2 cycles. (c) Ni K-edge XANES spectra for the $Li[Li_{1/6}Mn_{1/2}Ni_{1/6}Co_{1/6}]O_2$ compound during 2 cycles.

Fig. 9(a)–(c) shows the change in the valence states of Mn, Co and Ni ions, respectively, in the $Li[Li_{1/6}Mn_{1/2}Ni_{1/6}Co_{1/6}]O_2$ during two cycles and after fifty cycles. It is shown in Fig. 9(a) that the entire edge of the Mn K-edge XANES spectra does not change strictly to higher energy value during two cycles and after fifty cycles. As a result, the valence state of the Mn ions in the $Li[Li_{1/6}Mn_{1/2}Ni_{1/6}Co_{1/6}]O_2$ does not obviously change during the charge/discharge cycles. The shape of spectra after the first cycle (scan 4) differs from that of the fresh compound (pristine point, scan 0), it is similar, however, to that after fifty cycles. This indicates that the local structural changes of Mn ions are not clearly reversible during the first cycle, but that they are highly reversible after the first cycle. The redox behavior of the Co and Ni ions is clearly different from that of the Mn ions. As shown in Fig. 9(b) and (c), the oxidation states of the Co and Ni ions change reversibly as the cycles proceed. The valence state of the Co ions changes between Co^{3+} and $Co^{3.5+}$ while that of the Ni ions changes between Ni^{2+} and Ni^{3+}. Consequently, the redox behavior of the Co and Ni ions is highly reversible during the cycling process.

Considering the XANES results, it can be concluded that the redox reactions of Ni ($Ni^{2+}\leftrightarrow Ni^{3+}$) ions and Co ($Co^{3+}\leftrightarrow Co^{3.5+}$) are dominant at a 4.1 V plateau during charge/discharge cycles, whereas the valence state of Mn ions does not change.

4. Conclusions

As an alternative cathode material to $LiCoO_2$, $Li[Li_{1-x/3}Mn_{2-x/3}Ni_{x/3}Co_{x/3}]O_2$ powders ($x = 0.1$, 0.3, 0.5, 0.7 and 0.9) were investigated. The powders were synthesized easily using a sucrose combustion process. As a result of experiments using various compositions, the highest discharge capacity of 224 mAh/g was obtained at a composition of $x = 0.5$, as Li ions were used in place of heavy transition metal ions. When more Li_2MnO_3 exists compared to $Li[Ni_{1/3}Co_{1/3}Mn_{1/3}]O_2$, the discharge capacity is very low due to the electrochemically inactive Li_2MnO_3.

Via XANES spectra measurements, the electrochemical reaction of Ni and Co ions at 4.1 V ions is reversible during charge/discharge cycling. The local environmental change of Mn ions is irreversible during the first cycle, but becomes reversible after the first charge. The oxidation state of the Mn ions remains tetravalent during the cycling process. It is possible that this cathode material can be utilized for high capacity Li ion batteries

Acknowledgement

Experiments at PLS were supported in part by POSTECH.

References

[1] K. Ozawa, Solid State Ionics 69 (1994) 212.
[2] Y.S. Hong, Y.J. Park, K.S. Ryu, S.H. Chang, Y.J. Shin, J. Power Sources 147 (2005) 214.
[3] Z. Lu, D.D. MacNeil, J.R. Dahn, Electrochem. Solid-State Lett. 4 (12) (2001) A200.
[4] Y.J. Park, Y.S. Hong, X. Wu, K.S. Ryu, S.H. Chang, J. Power Sources 129 (2004) 288.
[5] S.H. Kang, K. Amine, J. Power Sources 124 (2003) 533.
[6] Z. Lu, L.Y. Beaulieu, R.A. Donaberger, C.L. Thomas, J.R. Dahn, J. Electrochem. Soc. 149 (2002) A778.
[7] A.D. Robertson, P.G. Bruce, Chem. Mater. 15 (2003) 1984.
[8] S.H. Kang, Y.K. Sun, K. Amine, Electrochem. Solid-State Lett. 6 (2003) A183.
[9] J. Choi, A. Manthiram, Electrochem. Solid-State Lett. 7 (10) (2004) A365.
[10] K.M. Shaju, G.V. Subba Rao, B.V.R. Chowdari, Electrochim. Acta 48 (2002) 145.
[11] M.M. Thackeray, S.-H. Kang, C.S. Johnson, VaugheyF J.T., R. Benedek, S.A. Hackney, J. Mater. Chem. 17 (2007) 3112.
[12] A. Yamada, S.C. Chung, K. Hinokuma, J. Electrochem. Soc. 148 (3) (2001) A224.
[13] P. Kalyani, S. Chitra, T. Mohan, S. Gopukumar, J. Power Sources 80 (1999) 103.
[14] Z. Lu, J.R. Dahn, J. Electrochem. Soc. 149 (7) (2002) A815.
[15] W.-S. Yoon, C.-P. Grey, M. Balasubramanian, X.-Q. Yang, M. James, Chem. Mater. 15 (2003) 3161.
[16] Y.J. Park, X. Wu, HongF Y.-S., K.S. Ryu, S.H. Chang, Solid State Ionics 175 (2004) 305.
[17] M. Balasubramanian, J. McBreen, I.J. Davidson, P.S. Whitfield, I. Kargina, J. Electrochem. Soc. 149 (2) (2002) A176.
[18] Y.J. Park, M.G. Kim, Y.-S. Hong, X. Wu, K.S. Ryu, S.H. Chang, Solid State Commun. 127 (2003) 509–514.
[19] B. Ammundsen, J. Paulsen, J. Adv. Mater. 13 (2001) 943.